Optics Letters

Photonic spin Hall effect in hyperbolic metamaterials at visible wavelengths

Osamu Takayama,[1,*] Johneph Sukham,[1] Radu Malureanu,[1] Andrei V. Lavrinenko,[1] and Graciana Puentes[2,3,4]

[1]DTU Fotonik, Department of Photonics Engineering, Technical University of Denmark, Ørsteds Plads 343, DK-2800 Kgs. Lyngby, Denmark
[2]Facultad de Ciencias Exactas y Naturales, Departamento de Física, Universidad de Buenos Aires, Buenos Aires, Argentina
[3]CONICET-Universidad de Buenos Aires, Instituto de Física de Buenos Aires (IFIBA), Buenos Aires, Argentina
[4]e-mail: gpuentes@df.uba.ar
*Corresponding author: otak@fotonik.dtu.dk

Received 23 July 2018; revised 28 August 2018; accepted 28 August 2018; posted 29 August 2018 (Doc. ID 340294); published 19 September 2018

The photonic spin Hall effect in transmission is a transverse beam shift of the out-coming beam depending on polarization of the incoming beam. The effect can be significantly enhanced by materials with high anisotropy. We report, to the best of our knowledge, the first experimental demonstration of the photonic spin Hall effect in a multilayer hyperbolic metamaterial at visible wavelengths (wavelengths of 520 and 633 nm). The metamaterial is composed of alternating layers of gold and alumina with deeply subwavelength thicknesses, exhibiting extremely large anisotropy. The angle-resolved polarimetric measurements showed the shift of 165 μm for the metamaterial of 176 nm in thickness. Additionally, the transverse beam shift is extremely sensitive to the variations of the incident angle changing theoretically by 270 μm with 1 milli-radian (0.057°). These features can lead to minituarized spin Hall switches and filters with high angular resolution.

OCIS codes: (160.3918) Metamaterials; (240.5440) Polarization-selective devices; (260.0260) Physical optics.

https://doi.org/10.1364/OL.43.004602

The photonic spin Hall effect [1] or spin Hall effect of light [2] is the photonic analog of the spin Hall effect occurring with charge carriers in solid-state systems. Typically, this phenomenon takes place when a light beam refracts at an air-glass interface, or when it is projected onto an oblique plane, the latter effect being known as the geometric spin Hall effect of light. In general, the photonic spin Hall effect leads to a polarization-dependent transverse shift of a light peak intensity [3–7]. An example of the latter effect is the transverse Imbert–Federov beam shift [8], which happens for paraxial beams reflected or refracted at a sharp inhomogeneity of an isotropic optical interface [6,7,9,10]. Potential applications of the photonic spin Hall effect in spin-dependent beam splitters, optical diodes [1], and surface sensors [11,12] are considered in various fields in photonics, such as nanophotonics, plasmonics, metamaterials, topological optics, and quantum optics [1,2].

The photonic spin Hall effect has been studied in reflection and transmission with various materials and geometrical settings. In the reflection configuration, the effect has been studied experimentally on the interfaces of uniaxial dielectrics ($LiNbO_3$) [13], glass prisms [14], metal (Ag) films [15], dielectric multilayers [16], and topological insulators [17]. In the case of the transmission configuration, the photonic spin Hall effect has been experimentally demonstrated in quartz crystals [18], anisotropic polymers [19], metal (Au) films [20], liquid crystals [21], and dielectric spheres [22].

Recently, metasurfaces and metamaterials, artificially engineered subwavelength surface and volume structures, have stimulated significant interest, thanks to their flexible design parameters [1]. A subclass of metamaterials—hyperbolic metamaterials (HMMs) exhibit extreme anisotropy with hyperbolic dispersions in the wavevector space. Conventionally, HMMs take the form of a multilayer of alternating metal and dielectric thin films [23,24], nanotrenches [25–27], or metallic nanowires [28]. In the typical cases, HMMs possess uniaxial anistropy, and their optical properties are characterized by effective ordinary and extraordinary permittivities, ε_o and ε_e, respectively, as depicted in Fig. 1. Depending on the sign of ε_o and ε_e, a metamaterial can be categorized as type I ($\varepsilon_o > 0$ and $\varepsilon_e < 0$) or type II HMM ($\varepsilon_o < 0$ and $\varepsilon_e > 0$) [29]. Such unique optical properties of HMMs have led to various applications, sub-diffraction imaging [30], and sensing [24,26,28]. The spin Hall effect in HMMs has been theoretically studied recently [31–33]. To the best of our knowledge, the experimental observation of the spin Hall effect in HMMs has been reported so far only for microwave frequencies [34]. The hyperbolic dispersion obtained with electronic components, such as capacitors and inductors, to steer directional surface waves [25,27,35,36] by input polarization states.

Here we experimentally demonstrate extreme angle sensitivity and enhancement of the spin Hall effect of light in HMMs in the visible regime. The effect is shown in the transmission configuration with a few hundreds of nanometers thick HMM

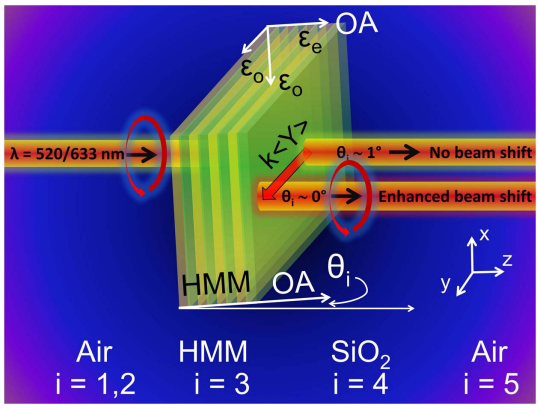

Fig. 1. Schematic illustration of the spin Hall effect. The transverse beam shift along the y-axis denoted as $\langle Y \rangle$ is switched by incident angle θ_i. The unit cell of the HMM structure consists of Al_2O_3 (10 nm)-APTMS (1 nm)-Au (10 nm)-APTMS (1 nm). The HMM contains eight periods with the total thickness of 176 nm. The optical axis of HMM is noted as OA.

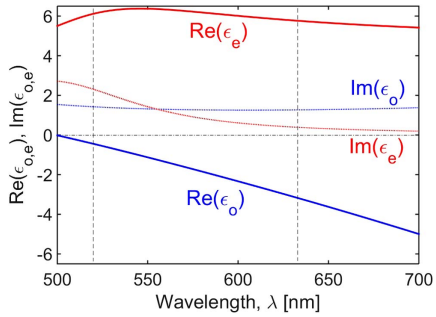

Fig. 2. Effective permittivities of multilayer HMM structure calculated by the effective media approximation. The wavelengths $\lambda =$ 520 nm and 633 nm at which we conducted experiments are noted by the vertical dashed lines.

composed of alternating layers of metal and dielectric, as illustrated in Fig. 1. The transverse beam shift in our HMM setting is very sensitive to the angle of incidence, drastically changing from almost no beam shift to a few hundred microns by the change of ≈0.003 rad (≈0.17°) in the incident angle. The large photonic spin Hall enhancement in a such thin structure and extreme angular sensitivity can be exploited in compact spin Hall devices which enable the manipulation of photons by polarization.

The HMM sample with the total thickness of 176 nm contains eight gold-alumina periods deposited on a 500 μm thick glass substrate. In particular, one period of the HMM structure consists of four layers: Al_2O_3 (10 nm), APTMS (1 nm), Au(10 nm), and APTMS (1 nm). APTMS, which stands for aminopropyl trimethoxysilane, is an almost loss-free adhesion layer advantageous for highly localized propagating plasmon modes [37]. The Au layer was sputtered, and the Al_2O_3 layer was deposited by atomic layer deposition. The treatment of HMMs as homogenized uniaxial media with effective permittivities is based on the effective media approximation [38], which is assumed to be valid under the condition that the thicknesses of individual layers are deeply subwavelength. The unit cell is $\Lambda = 22$ nm, and normalized by the wavelength interval of $\lambda = 500$–700 nm, provides the ratio of $\Lambda/\lambda = 1/22.7$–$1/31.8$. Thus, the application of the effective media approximation in our case is justified [38].

The ordinary and extraordinary permitivities of the HMM, denoted as ε_o and ε_e, respectively, are calculated as [39]

$$\varepsilon_o = f_{\mathrm{Au}} \cdot \varepsilon_{\mathrm{Au}} + f_{\mathrm{Al_2O_3}} \cdot \varepsilon_{\mathrm{Al_2O_3}} + f_{\mathrm{APTMS}} \cdot \varepsilon_{d_{\mathrm{APTMS}}}, \quad (1)$$

$$\varepsilon_e = \left(\frac{f_{\mathrm{Au}}}{\varepsilon_{\mathrm{Au}}} + \frac{f_{\mathrm{Al_2O_3}}}{\varepsilon_{\mathrm{Al_2O_3}}} + \frac{f_{\mathrm{APTMS}}}{\varepsilon_{\mathrm{APTMS}}} \right)^{-1}, \quad (2)$$

where ε_m and ε_d are the permittivities of metal and dielectric, and f_m and f_d are the volume fractions of metal and dielectric, respectively. The permittivity of the Au film, ε_m, is characterized by the Drude–Lorentz model with the thickness-dependent correction [37]. The refractive index of APTMS is 1.46 [40]. Figure 2 shows dispersion of the HMM effective permittivities in the visible range. Our HMM structure has a zero crossing wavelength for ε_o around $\lambda = 500$ nm and, further to the red wavelengths, becomes type II HMMs ($\varepsilon_o < 0$ and $\varepsilon_e > 0$).

In order to understand the behavior of the spin Hall beam shift in HMMs, we conducted a simulation based on a theory developed by Tang *et al.* [32,33] with realistic parameters of fabricated HMMs presented in Fig. 2. The whole HMM-SiO_2 substrate structure has air as the ambient medium, as shown in Fig. 1. We assume that the incident light is impinging on the HMM structure in the y-z plane with incident angle θ_i. The relative permittivities of the media in regions 1–5 are denoted by $\varepsilon_i (i = 1, 2, 3, 4, 5)$, respectively [32], where $\varepsilon_1 = \varepsilon_2 = \varepsilon_5 = 1$ (air), ε_4 corresponds to the SiO_2 substrate, and ε_3 corresponds to the HMM. The HMM is assumed to be nonmagnetic and uniaxial anisotropic with a relative permittivity tensor (ε_3):

$$\varepsilon_3 = \begin{pmatrix} \varepsilon_o & 0 & 0 \\ 0 & \varepsilon_o & 0 \\ 0 & 0 & \varepsilon_e \end{pmatrix}. \quad (3)$$

Considering the input Gaussian beam of waist ω_0,

$$E_{H,V}(x, y) = \frac{\omega_0}{\sqrt{2\pi}} \exp - \frac{\omega_0^2 (k_x^2 + k_y^2)}{4}, \quad (4)$$

we can define the transverse beam shifts after transmission through the structure in the form

$$\eta_{H,V}^{\pm} = \frac{\iint x |E_{H,V}|^{\pm} \mathrm{d}x\mathrm{d}y}{\iint |E_{H,V}|^{\pm} \mathrm{d}x\mathrm{d}y}, \quad (5)$$

where $\eta^{\pm}$ indicate transverse shifts for the right-hand circular (RHC) and left-hand circular polarizations. The transverse shifts include z-dependent and z-independent terms which represent spatial and angular transverse shifts, respectively [32]. Here we focus on the spatial transverse shift of transmitted light through the HMM waveguide, which takes the form [32]

$$\langle Y \rangle = \pm \frac{k_1 \omega_0^2 \left(t_s^2 \frac{\cos(\theta_t)}{\sin(\theta_i)} - t_s t_p \cot(\theta_i) \right)}{k_1^2 \omega_0^2 t_s^2 + \cos^2(\theta_i) \left(t_s \frac{\cos(\theta_t)}{\cos(\theta_i)} - t_p \right)^2 + \left(\frac{dt_s}{d\theta_i} \right)^2}, \quad (6)$$

where $k_1 = n_1 k = n_1 \frac{2\pi}{\lambda}$ with $n_1 = 1$ (air); $t_{s,p}$ are the transmission amplitudes for the s, p modes, respectively [32]; and θ_t is the transmission angle. We consider $(\frac{dt_s}{d\theta_i}) \approx 0$ for a large

beam waist and $\theta_t = 0$, assuming transmission along the laser beam axis.

To demonstrate the angular sensitivity of the photonic spin Hall shift in the HMM, we performed a series of characterizations using the polarimetric setup shown in Fig. 3. The transverse beam shift can be measured by polarimetric and quantum weak measurements [18,19,41]. As a source of an incident Gaussian beam, we employed a He-Ne laser with a wavelength $\lambda = 633$ nm and a diode laser with a wavelength $\lambda = 520$ nm. The laser radiation was collimated using a microscope objective lens. We measured the anisotropic phase difference Φ_0 versus angle θ_i with the Stokes polarimetry method [18]. The input polarization state (RHC) is prepared using a quarter-wave plate (QWP) followed by a Glan–Thompson polarized (P1). The phase difference can be obtained via the Stokes parameters using the expression

$$\Phi_0 = \arctan(S_3/S_2), \tag{7}$$

where $S_3 = I(90°, 45°) - I(90°, 135°)$ is the normalized Stokes parameter for the circular polarization, and $S_2 = I(0°, 45°) - I(0°, 135°)$ is the normalized Stokes parameter in the diagonal basis, where the normalization factor S_0 is given by the total intensity of the beam. δ and α of $I(\delta, \alpha)$ correspond to the retardation angle of QWP2 and the rotation angle of polarizer P2, respectively. The measured phase using Eq. (7) is wrapped in the range $(-\pi, \pi)$. In order to determine the unwrapped phase difference, we use the unwrapping algorithm [18] with a tolerance set to 0.01 rad.

The transverse beam shift, $\langle Y \rangle$, is found from the measured phase, Φ_0 [18]:

$$\langle Y \rangle = \frac{1}{k} \cot(\pi/2 - \theta_i)[-\sigma(1 - \cos \Phi_0) + \chi \sin \Phi_0], \tag{8}$$

where σ and χ are the Stokes parameters in the circular and diagonal basis, respectively. They are given by $\sigma = 2\,\mathrm{Im}(\alpha^*\beta)$ and $\chi = 2\,\mathrm{Re}(\alpha^*\beta)$ from the Jones vector $|\psi\rangle = \binom{\alpha}{\beta}$ of the incident beam, respectively. The incident beam has the RHC polarization; that is, $\alpha = \frac{1}{\sqrt{2}}$, $\beta = \frac{i}{\sqrt{2}}$.

Figure 4 shows the experimental points of the beam shifts for wavelengths $\lambda = 520$ nm and $\lambda = 633$ nm versus the simulated results, where losses of the HMM were taken into account. The effective permittivitties are $\varepsilon_o = -2.94 + 1.21i$ and $\varepsilon_e = 5.50 + 0.33i$ for $\lambda = 633$ nm, and $\varepsilon_o = -0.32 + 1.36i$ and $\varepsilon_e = 5.88 + 1.99i$ for $\lambda = 520$ nm, respectively (see Fig. 2). The simulation results in Figs. 4(a) and 4(b) are fitted in terms of beam width w_o. Note that the inset in Fig. 4(a) is the simulated transmittance of unpolarized incident light. We also measured the transmittance of unpolarized normal incident light in the same wavelength range, yielding the transmittance from 0.2% to a few percent. Here we can observe the peculiarities of the photonic spin Hall effect in HMM structures in the transmission configuration. The transverse beam shift in HMMs is extremely sensitive to the incident angle: its variation from $\theta_i = 0$ rad to merely $\theta_i = 0.003$ rad (0.17°) for $\lambda = 633$ nm [Fig. 4(a)] induces the giant beam shift of a few hundreds of microns, exhibiting sensitivity in the milliradian range. The angular variation from $\theta_i = 0.003$ rad to above also significantly changes the beam shift from $\langle Y \rangle = 105$ μm to merely $\langle Y \rangle = 10$ μm, which is almost one order of magnitude difference [Fig. 4(a)]. The sharp peak of the beam shift is attributed to large anisotropy of HMMs, $\varepsilon_e - \varepsilon_o$; we also saw such behavior in dielectric media [19]. As shown by the simulated results in Fig. 4(a) and the inset of Fig. 4(b), the transverse beam shift is larger for $\lambda = 633$ nm with larger anisotropy than the $\lambda = 520$ nm case for the same beam width $w_o = 100$ μm. For $\lambda = 520$ nm with a larger beam diameter [Fig. 4(b)], the beams shift exhibits even sharper resonance and, consequently, enhanced angular sensitivity: the peak shift of $\langle Y \rangle = 270$ μm is achieved by the incident angle change of 0.001 rad (0.057°) only (≈4700 μm/°). When the incident angle becomes larger, for instance, $\theta_i = 0.01$ rad (0.57°), the beam shift drastically drops to $\langle Y \rangle = 10$ μm and less.

The experimental results are in the full quantitative agreement with the simulated values, taking into account beam divergence and setup errors. The beam divergence of the He-Ne laser is estimated to be about $\Delta\theta_i = 0.01$ rad (0.57°),

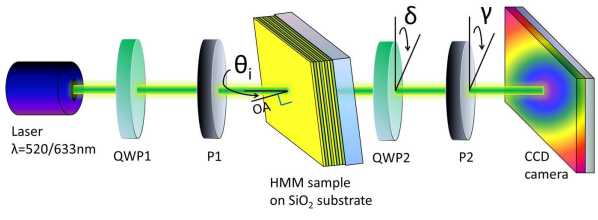

Fig. 3. Schematic illustration of polarimetric measurement setup. P1 and P2 represent double Glan-Laser polarizers; QWP1 and QWP2 are quarter-wave plates. The laser is either a He–Ne laser or a diode laser with a wavelength of 633 and 520 nm, respectively. The optical axis of HMM is noted as OA.

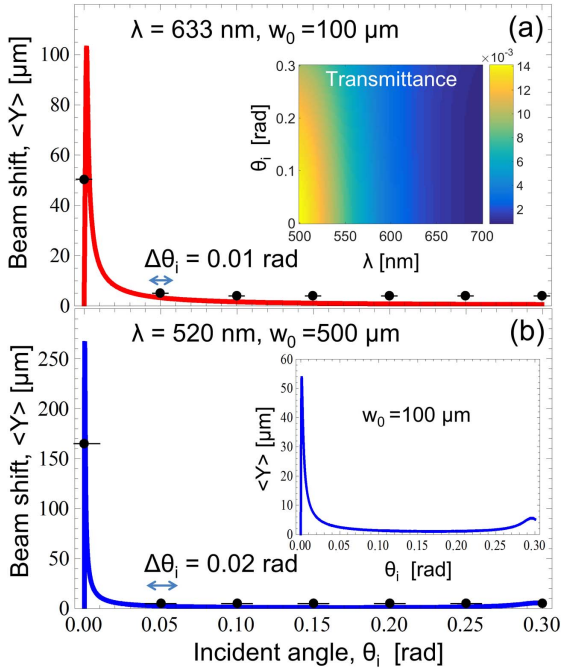

Fig. 4. Measured and simulated (solid lines) spin Hall transverse shift, $\langle Y \rangle$, for (a) $\lambda = 633$ nm and (b) $\lambda = 520$ nm. Note that there is an estimated beam divergence of $\Delta\theta_i = 0.01$ rad for $\lambda = 633$ nm and $\Delta\theta_i = 0.02$ rad for $\lambda = 520$ nm, indicated as lateral error bars. The inset in (a) is the transmittance through the HMM calculated by a scattering matrix method [42], and the inset in (b) is the simulated beam shift for $w_o = 100$ μm.

and the beam divergence of the green diode laser is about $\Delta\theta_i = 0.02$ rad (1.14°). Additionally, the angular resolution is limited by the rotating mount with an error of about 0.0017 rad (0.1°). For $\lambda = 633$ nm [Fig. 4(a)], the experimental transverse beam shift under the normal incidence reaches $\langle Y \rangle = 50$ μm. However, when the incident angle is tilted by merely $\theta_i = 0.035$ rad (≈2°), the transverse beam shift dramatically drops to $\langle Y \rangle = 5$ μm. Such results confirm that the transverse beam shift can be tuned within one order of magnitude range by small angular variations demonstrating extreme angular sensitivity of the spin Hall effect in HMMs. The waist used for the simulations ($w_0 = 100$ μm) is measured experimentally.

In the case of $\lambda = 520$ nm, we observe $\langle Y \rangle = 165$ μm for $\theta_i = 0$ rad, as shown in Fig. 4(b). At $\theta_i = 0.035$ rad (≈2°), the beam shift decreases to $\langle Y \rangle = 5$ μm. This extremely high angular sensitivity makes a striking contrast to the previously observed spin Hall effect in dielectric anisotropic media, such as a quartz crystal (≈150 μm/5° = 30 μm/°) [18] and polymer film (≈250 μm/20° = 12.5 μm/°) [19], where the beam shift of the same magnitude occurs within several degrees of sample tilting, which is two orders of magnitude larger. Moreover, the thickness of the HMM is 176 nm only, as opposed to those of the dielectric materials: 50 μm for the polymer film and 1 mm for the quartz plate. In contrast to isotropic media, the photonic spin Hall effect on anisotropic media exhibits larger beam shift when the anisotropy becomes larger. It works for both dielectric media [19] and HMMs with even larger anisotropy [32,33]. This enables us to enhance and tune the transverse beam shift by anisotropy.

In conclusion, we experimentally demonstrated for the first time, to the best of our knowledge, the photonic spin Hall effect in a HMM at visible wavelengths. The transverse beam shift in the transmission configuration is very sensitive to the incident angle: we observed that a few milli-radian difference changes the beam shift by two orders of magnitude, for example, from a few hundreds of microns down to several microns. This extreme angular tunability is realized in a 200 nm thick HMM. Such sensitivity can lead to thin and compact spin Hall devices that manipulate light at nanoscale by means of spin, incident angle, and wavelength, such as switches, filters, and sensors.

Funding. Agencia Nacional de Promoción Científica y Tecnológica (ANPCyT) (PICT2015-0710 Startup, UBACyT PDE 2016, UBACyT PDE 2017); Villum Fonden (11116); Direktør Ib Henriksens Fond.

Acknowledgment. The authors are grateful to Konstantin Bliokh, Mark Dennis, and Joerg Goette for fruitful discussions.

REFERENCES

1. Y. Liu, Y. Ke, H. Luo, and S. Wen, Nanophotonics **6**, 51 (2017).
2. X. Ling, X. Zhou, K. Huang, Y. Liu, C.-W. Qiu, H. Luo, and S. Wen, Rep. Prog. Phys. **80**, 066401 (2017).
3. N. B. Baranov, A. Y. Savchenko, and B. Y. Zel'dovich, J. Exp. Theor. Phys. Lett. **59**, 232 (1994).
4. Z. Bomzon, G. Biener, V. Kleiner, and E. Hasman, Opt. Lett. **27**, 1141 (2002).
5. K. Y. Bliokh, Phys. Rev. Lett. **97**, 043901 (2006).
6. K. Y. Bliokh, A. Niv, V. Kleiner, and E. Hasman, Nat. Photonics **2**, 748 (2008).
7. A. Aiello and J. P. Woerdman, Opt. Lett. **33**, 1437 (2008).
8. K. Y. Bliokh and A. Aiello, J. Opt. **15**, 014001 (2013).
9. K. Y. Bliokh, F. J. Rodríguez-Fortuño, F. Nori, and A. V. Zayats, Nat. Photonics **9**, 796 (2015).
10. F. Cardano and L. Marrucci, Nat. Photonics **9**, 776 (2015).
11. X. Zhou, X. Ling, H. Luo, and S. Wen, Appl. Phys. Lett. **101**, 251602 (2012).
12. X. Zhou, L. Sheng, and X. Ling, Sci. Rep. **8**, 1221 (2018).
13. Y. Qin, Y. Li, X. Feng, Z. Liu, H. He, Y.-F. Xiao, and Q. Gong, Opt. Express **18**, 16832 (2010).
14. Y. Qin, Y. Li, H. He, and Q. Gong, Opt. Lett. **34**, 2551 (2009).
15. X. Zhou, Z. Xiao, H. Luo, and S. Wen, Phys. Rev. A **85**, 043809 (2012).
16. B. Wang, Y. Li, M. M. Pan, J. L. Ren, Y. F. Xiao, H. Yang, and Q. Gong, Phys. Rev. A **88**, 043842 (2013).
17. X. Zhou, J. Zhang, X. Ling, S. Chen, H. Luo, and S. Wen, Phys. Rev. A **88**, 053840 (2013).
18. K. Y. Bliokh, C. T. Samlan, C. Prajapati, G. Puentes, N. K. Viswanathan, and F. Nori, Optica **3**, 1039 (2016).
19. O. Takayama and G. Puentes, Opt. Lett. **43**, 1343 (2018).
20. X. Zhou, X. Ling, Z. Zhang, H. Luo, and S. Wen, Sci. Rep. **4**, 7388 (2014).
21. L. Marrucci, C. Manzo, and D. Paparo, Phys. Rev. Lett. **96**, 163905 (2006).
22. D. Haefner, S. Sukhov, and A. Dogariu, Phys. Rev. Lett. **102**, 123903 (2009).
23. A. J. Hoffman, L. Alekseyev, E. E. Narimanov, C. Gmachl, and D. L. Sivco, Nat. Mater. **6**, 946 (2007).
24. K. V. Sreekanth, Y. Alapan, M. ElKabbash, E. Ilker, M. Hinczewski, U. A. Gurkan, A. De Luca, and G. Strangi, Nat. Mater. **15**, 621 (2016).
25. O. Takayama, E. Shkondin, A. Bogdanov, M. E. Aryaee Pahah, K. Golenitskii, P. A. Dmitriev, T. Repän, R. Malreanu, P. Belov, F. Jensen, and A. V. Lavrinenko, ACS Photon. **4**, 2899 (2017).
26. E. Shkondin, T. Repän, M. E. Aryaee Panah, A. V. Lavrinenko, and O. Takayama, ACS Appl. Nano Mater. **1**, 1212 (2018).
27. O. Takayama, P. Dmitriev, E. Shkondin, O. Yermakov, M. E. A. Panah, K. Golenitskii, F. Jensen, A. Bogdanov, and A. V. Lavrinenko, Semiconductors **52**, 442 (2018).
28. V. Kabashin, P. Evans, S. Pastkovsky, W. Hendren, G. Wurtz, R. Atkinson, R. Pollard, V. Podolskiy, and V. Zayats, Nat. Mater. **8**, 867 (2009).
29. Y. Guo, W. Newman, C. L. Cortes, and Z. Jacob, Adv. OptoElectron. **2012**, 452502 (2012).
30. D. Lu and Z. Liu, Nat. Commun. **3**, 1205 (2012).
31. O. Y. Yermakov, A. I. Ovcharenko, A. A. Bogdanov, I. V. Iorsh, K. Y. Bliokh, and Y. S. Kivshar, Phys. Rev. B **94**, 075446 (2016).
32. T. Tang, C. Li, and L. Luo, Sci. Rep. **6**, 30762 (2016).
33. T. Tang, Y. Zhang, J. Li, and L. Luo, IEEE Photon. J. **9**, 4600910 (2017).
34. P. V. Kapitanova, P. Ginzburg, F. J. Rodríguez-Fortuño, D. S. Filonov, P. M. Voroshilov, P. Belov, A. N. Poddubny, Y. S. Kivshar, G. Wurtz, and A. V. Zayats, Nat. Commun. **5**, 3226 (2014).
35. O. Takayama, A. Bogdanov, and A. V. Lavrinenko, J. Phys. **29**, 463001 (2017).
36. I. S. Sinev, A. A. Bogdanov, F. E. Komissarenko, K. S. Frizyuk, M. I. Petrov, I. S. Mukhin, S. V. Makarov, A. K. Samusev, A. V. Lavrinenko, and I. V. Iorsh, Laser Photon. Rev. **11**, 1700168 (2017).
37. J. Sukham, O. Takayama, A. Lavrinenko, and R. Malureanu, ACS Appl. Mater. Interfaces **9**, 25049 (2017).
38. L. Ferrari, C. Wu, D. Lepage, X. Zhang, and Z. Liu, Prog. Quantum Electron. **40**, 1 (2015).
39. A. Lavrinenko and V. Zhilko, Microw. Opt. Technol. Lett. **15**, 54 (1997).
40. L. Brigo, E. Gazzola, M. Cittadini, P. Zilio, and G. Zacco, Nanotechnology **24**, 155502 (2013).
41. G. Puentes, N. Hermosa, and J. Torres, Phys. Rev. Lett. **109**, 1 (2012).
42. D. Y. K. Ko and J. R. Sambles, J. Opt. Soc. Am. A **5**, 1863 (1988).